WP2.11 Cal/Val BC006.2
Final Report

Reference: CLS-ENVP-RP-25-0237

Issue: 1.1

Date: December 12, 2025

Contract: COPAS_460000262

This content has been intentionally removed

Change Log

Version	Date	Changes
1.0	December 8, 2025	First Draft
1.1	December 12, 2025	Final version

Table of Content

1 Introduction **8**

2 Data and Methods **8**
2.1. Sentinel-3 data . . . 8
2.2. Processing Baseline BC006.02 . . . 8
2.3. Data editing . . . 9
2.4. Cal/Val analysis . . . 9

3 Results: Open-ocean **10**
3.1. Dataset availability and data validity . . . 10
3.2. Range . . . 11
3.3. Sigma0 . . . 13
3.4. Significant Wave Height . . . 14
3.5. Sea Surface Height Anomaly . . . 15
3.6. Spectral Analysis . . . 17

4 Results: Polar regions **18**
4.1. Leads detection . . . 19
4.2. Sea Level Anomaly . . . 20
4.3. Open ocean/lead bias . . . 22

5 Conclusions **23**

List of Figures

1 Editing parameters and thresholds used in the cal/val analysis. 9

2 Geobox maps of mean percentage of edited observations by thresholds between June 2020 and June 2022 for BC005.02 (left) and BC006.02 (right) 11

3 Geobox maps of mean difference between BC006.02 and BC005.02 in the number of 20 Hz observations used in compression to 1 Hz. 11

4 Range difference between BC006.02 and BC005.02 for Synthetic Aperture Radar (SAR) (top) and Pseudo Low Resolution Mode (PLRM) (bottom). Left column: geobox maps of mean difference from June 2020 and June 2022. Right column: time series of mean difference per day (blue) and per pass (red). 12

5 Geobox map of difference in range standard deviation between BC006.02 and BC005.02. As for the mean from the previous figures, the standard deviation is computed over boxes of 2° by 2° for the period June 2020 to June 2022. 12

6 Sigma0 difference between BC006.02 and BC005.02 for SAR (top) and PLRM (bottom). Left column: geobox maps of mean difference from June 2020 and June 2022. Right column: time series of mean difference per day (blue) and per pass (red). 13

7 Geobox maps of the mean mode difference (i.e. SAR minus PLRM) of sigma0 for BC005.02 (left) and BC006.02 (right). 14

8 Significant Wave Height (SWH) difference between BC006.02 and BC005.02 for SAR (top) and PLRM (bottom). Left column: geobox maps of mean difference from June 2020 and June 2022. Right column: time series of mean difference per day (blue) and per pass (red). . 14

9 Geobox maps of the mean processing-mode difference (i.e. SAR minus PLRM) of SWH for BC005.02 (left) and BC006.02 (right). 15

10 Sea Surface Height Anomaly (SSHA) difference between BC006.02 and BC005.02 for SAR (top) and PLRM (bottom). Left column: geobox maps of mean difference from June 2020 and June 2022. Right column: time series of mean difference per day (blue) and per pass (red). 16

11 Geobox maps of the mean mode difference (i.e. SAR minus PLRM) of SSHA for BC005.02 (left) and BC006.02 (right). 16

12 Geobox maps of the mean difference between ascending and descending passes of the mode difference (i.e. SAR minus PLRM) of SSHA for BC005.02 (left) and BC006.02 (right). . 16

13 Geobox maps of mean SAR SSHA difference at crossovers between Sentinel-3A and Jason-3 for BC005.02 (left) and BC006.02 (right). The differences were computed only for crossing tracks less than 10 days apart. 17

14 Time series of Sentinel-3 (BC005.02 in light red; BC006.02 in dark red), Sentinel-6A (LR_NR mode in green; HR mode in black) and Jason-3 SSHA (gray). The dots correspond to daily averages; the lines to 30-day moving averages. Sentinel-3 PLRM curves show values analogous to SAR and thus are not shown for figure clarity. 17

15 SSHA power density spectra for 1 Hz (left) and 20 Hz observations (right). 18

16 SWH power density spectra for 1 Hz (left) and 20 Hz observations (right). 18

17 Ice lead analysis in the Arctic (top) and Antarctic regions (bottom). Left column: time-series of daily number of detected leads for BC005.02 (orange), BC006.02 based on the same flag (light green) and BC006.02 based on the new waveform classification flag (dark green). Right column: Geobox maps of the difference in the percentage of leads detected within each box between BC006.02 and BC005.02. 19

18 Time series of daily mean SSHA for the Arctic (left column) and Antarctic regions (right column). Top: time-series for BC005.02 (orange) and BC006.02 (green). Bottom: same time series as top but also compared to CryoTEMPO (cyan) and SARAL/AltiKa SSHA (purple). . 20

19 Geobox maps of average SSHA in the Arctic (top) and the Antarctic region (bottom). Left column: BC005.02; Middle column: BC006.02; Right column: CryoTEMPO. 21

20 Geobox maps of standard deviation of SSHA in the Arctic (top) and the Antarctic region (bottom). Left column: BC005.02; Middle column: BC006.02; Right column: CryoTEMPO. . 21

21 Geobox maps of open-ocean/lead SSHA bias in the Arctic (top) and the Antarctic region (bottom). Left column: BC005.02; Right column: BC006.02. 22

22 Time-series of mean open-ocean/lead SSHA bias per cycle for the Arctic (left) and the Antarctic regions (right). BC005.02 is in orange; BC006.02 is in green. 23

Acronyms

CMEMS	Copernicus Marine Services.
ECMWF	European Centre for Medium-Range Weather Forecasts.
MSS	Mean Sea Surface.
NRT	Near real time.
NTC	Non time critical.
PB	Processing Baseline.
PLRM	Pseudo Low Resolution Mode.
PTR	Point Target Response.
RMS	Root Mean Square.
SAR	Synthetic Aperture Radar.
SSHA	Sea Surface Height Anomaly.
STC	Short time critical.
SWH	Significant Wave Height.
TDS	test dataset.

1 Introduction

The goal of this study is to perform a scientific validation of the data quality (cal/val) of the new Sentinel-3 Processing Baseline (PB) BC006.02 against the previous reference baseline BC005.02 that in 2023 was used for a full reprocessing (i.e. from the beginning of the missions) of Sentinel-3A/-3B data. The new PB BC006.02 has been implemented by EUMETSAT to satisfy the needs from the Copernicus Marine Services (CMEMS) over polar ocean (northern and southern): specifically, to significantly improve the overall data quality and to ensure the sea level continuity between the open ocean and polar ocean regions.

2 Data and Methods

2.1. Sentinel-3 data

The analysis has been based on a pre-operational BC006.02 test dataset (TDS) specifically produced by EUMETSAT for this work-package. The TDS includes only Sentinel-3A observations, spanning a 2-year period from mid-2020 (cycle 58, pass 740) to mid-2022 (cycle 87, pass 175). Unless stated otherwise, the data used for the global analysis are 1 Hz NTC observations. 20 Hz observations have been primarily used for the polar region analysis.

The dataset used as the baseline reference for this study is the operational dataset processed under PB BC.005.02. Although more recent PB are currently available, the temporal period for the analysis was chosen specifically to have a homogeneous reference dataset in BC005.02. A detailed description of BC005.02 specifications can be found in its product notice [1]. In terms of geophysical corrections, they are the ones from the equivalent GDR-F standard. In particular, the Mean Sea Surface (MSS) used in the BC005.02 is the combined MSS, CNES/CLS15, SIO, DTU15[1].

2.2. Processing Baseline BC006.02

The BC006.02 evolutions at level 1 include:

- Range Walk CZT [2]
- New Spectral Weighting Window [3]
- Waveform Zero-Padding [4]
- Fast Time Complex Calibration [5]
- Dynamic AutoCal [6]
- L1B masking
- Updated Sigma0 bias

and at level 2:

- GDR-G standards for geophysical corrections (operational since BC006.01 [7])
- SAMOSA+ Waveform Retracker [8]
- Waveform Classification [9]

[1] https://doi.org/10.24400/527896/a01-2021.004

- SWH Correction for Vertical Wave Motion [10] (the LUT takes as input two SAR-based parameters: wave period (T02) and standard deviation of vertical wave velocity (σ_v)[11])
- New Sea State Bias Solution (to correct for meridional wind concentration) [12]
- OSISAF sea ice concentration (implemented since PB.005.03) [13]
- Waves from MeteoFrance model
- Upper threshold for SWH updated to 25 m (instead of 15 m) [14]

2.3. Data editing

The first step of the cal/val analysis consisted in quantifying the number of missing and invalid measurements. Missing measurements correspond to gaps along the satellite track during which no satellite observations were retrieved. Invalid measurements include retrieved observations for which values of certain measured parameters are outside a given threshold interval. The process of removing invalid observations is called data editing.

In our analysis, the editing procedure is the same one as used for other COPAS cal/val reports. Invalid measurements are detected over all ice-free, open-ocean observations by applying a series of maximum and minimum thresholds on various parameters. A measurement is edited if at least one parameter is found to be outside those thresholds. A complete list of the parameters used for data editing and their associated thresholds is provided in the table in Figure 1.

	SAR	PLRM
ssh	[-130 ; 100] m	[-130 ; 100] m
ssha	[-2 ; 2] m	[-2 ; 2] m
range_number	[10 ; +∞]	[10 ; +∞]
range_std	[0 ; 0.12+0.02*swh] m	[0 ; 0.18+0.015*swh] m
sigma0	[5 ; 28] dB	[5 ; 28] dB
sigma0_std	[0 ; 0.7] dB	[0 ; 0.7] dB
swh	[0 ; 15] m	[0 ; 15] m
wind_speed	[0 ; 30] m/s	[0 ; 30] m/s
sea_state_bias	[-0.5 ; 0] m	[-0.5 ; 0] m
ionospheric_corr	[-0.4 ; 0.04] m	[-0.4 ; 0.04] m
dry_tropo_corr	[-2.5 ; -1.9] m	[-2.5 ; -1.9] m
ocean_tide	[-5 ; 5] m	[-5 ; 5] m
pole_tide	[-15 ; 15] m	[-15 ; 15] m
solid_earth_tide	[-1 ; 1] m	[-1 ; 1] m
wet_tropo_corr	[-0.5 ; -0.001] m	[-0.5 ; -0.001] m
DAC	[-2 ; 2] m	[-2 ; 2] m

Figure 1: Editing parameters and thresholds used in the cal/val analysis.

2.4. Cal/Val analysis

The scientific validation was designed around two main goals:

1. Assess non-regression over open ocean regions
2. Assess data quality enhancements over polar regions

Ultimately, the validation results were used to confirm whether the continuity between open ocean and polar ocean regions is achieved, as requested by CMEMS.

The diagnostics investigated for the cal/val analysis include:

- Time-series: mean and variance computed per-day and per-track
- Geobox maps: maps of mean values computed over 2° longitude by 2° latitude boxes
- Power density spectra: computed over continuous segments of 2000 km
- Cross-over differences: visualized as both time series and geobox maps of mean and variance

These diagnostics were computed for both SAR mode and PLRM and then compared between BC005.02 and BC006.02. Diagnostics of mode differences (e.g. SAR-PLRM) were also computed and compared between the two baselines. In case of wind and waves, the data quality was also assessed with respect to the European Centre for Medium-Range Weather Forecasts (ECMWF) weather forecast model. Cross-over analysis included mono-mission as well as multi-mission differences. Jason-3 was used for the non-regression over open-ocean analysis; CryoSat-2 (specifically the CryoTEMPO polar ocean thematic product[2]) and SARAL/AltiKa (GDR-F standards) for the polar analysis.

The analysis investigated several variables available from the products. Here we present the results for the main variables (i.e. range, sigma0, SWH, SSHA), but similar analysis was performed also for wind, ionospheric path delay, wet-tropospheric corrections and sea state bias.

For the assessment in the polar oceans, the validation focused on the new dedicated SSHA field which uses specific geophysical corrections for the polar regions (variable polar_ocean_20_ku in the products). Additionally, the analysis included an assessment on leads detection. These were identified via a new dedicated sea-ice lead flag included in the products (variable surf_type_class_wfc_20_ku).

3 Results: Open-ocean

The first part of the cal/val activities consisted in assessing the quality of BC006.02 over open ocean to ensure that the changes introduced to improve the performance in polar areas did not degrade the performance at lower latitudes.

3.1. Dataset availability and data validity

The analysis of missing observations returned nominal results, showing no major variations between the two baseline collections in the period from June 2020 to June 2022. The analysis of edited observations, however, showed pronounced differences between the two (Figure 2).

In the polar regions, BC006.02 showed a substantially lower percentage of edited measurements than BC005.02. This was expected, since the large number of edited observations in BC005.02, resulted from a bug in the open sea ice flag that was already fixed before BC006.02. On the other hand, in the tropical band between 30°N and 30°S, BC006.02 showed a slightly larger percentage of edited measurement (with max differences of around 10% more).

A detailed analysis of the editing flags indicated that higher values of the Root Mean Square (RMS) of sigma0 (computed from the 20Hz observations used to derive the 1Hz value) were responsible for the increased number of edited measurements. The reason for this increase in RMS of sigma0 was identified in a bug introduced in the retracking step of the new processing chain which relaxed the conditions for which outliers observations at 20 Hz are identified and removed before the 1 Hz compression. Since this

[2] https://www.cpom.ucl.ac.uk/cryotempo/index.php?theme=polaroceans

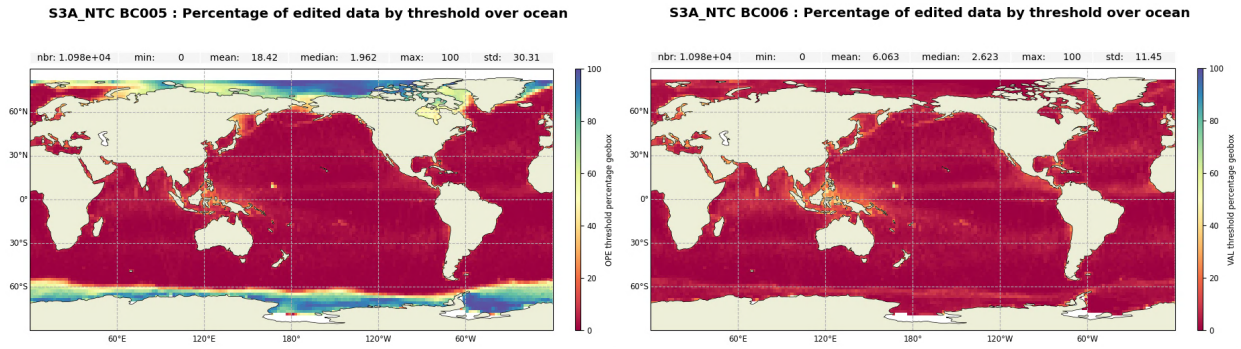

Figure 2: Geobox maps of mean percentage of edited observations by thresholds between June 2020 and June 2022 for BC005.02 (left) and BC006.02 (right)

preliminary analysis, the bug has been understood and will be corrected in the version of the BC006 which will be deployed for production.

Our cal/val analysis was performed on the BC006.02 TDS impacted by the bug. Although, the editing step removed a large portion of 1 Hz measurements impacted by 20 Hz outliers, some valid measurements were possibly impacted by them. A map of the difference in the number of 20 Hz observations used in compression (Figure 3) shows that overall BC006.02 1 Hz observations are reconstructed using a larger number of 20 Hz measurements than in BC005.02. The geographical distribution of the positive differences is consistent with the patterns of higher percentage of edited observations observed in Figure 2, indicating that the two result from the same bug.

For our analysis, we accepted that the resulting valid 1 Hz measurements in the impacted regions might be slightly degraded (i.e. noisier). However, as shown by our results in the following sections, the bug had ultimately negligible impact in the overall performance of BC006.02.

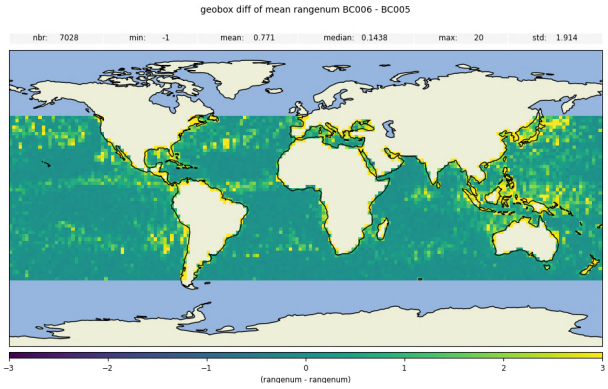

Figure 3: Geobox maps of mean difference between BC006.02 and BC005.02 in the number of 20 Hz observations used in compression to 1 Hz.

3.2. Range

Range analysis showed BC006.02 values consistent with those from BC005.02 (Figure 4). A constant bias of roughly 5 mm is observed in SAR mode. The geographical distribution of the differences is homogeneous and their temporal evolution is stable. PLRM shows a slightly larger bias (around 6 mm), with differences between the two baselines more pronounced at high latitudes. The time series is characterized by a small positive trend and high frequency oscillations of small amplitude. Further studies will be required to better understand their origin and significance.

A clear improvement in BC006.02 is a reduced variability (random noise) in range values. Comparison with BC005.05 revealed that the reduced variability is characterized by geographical patterns likely associated

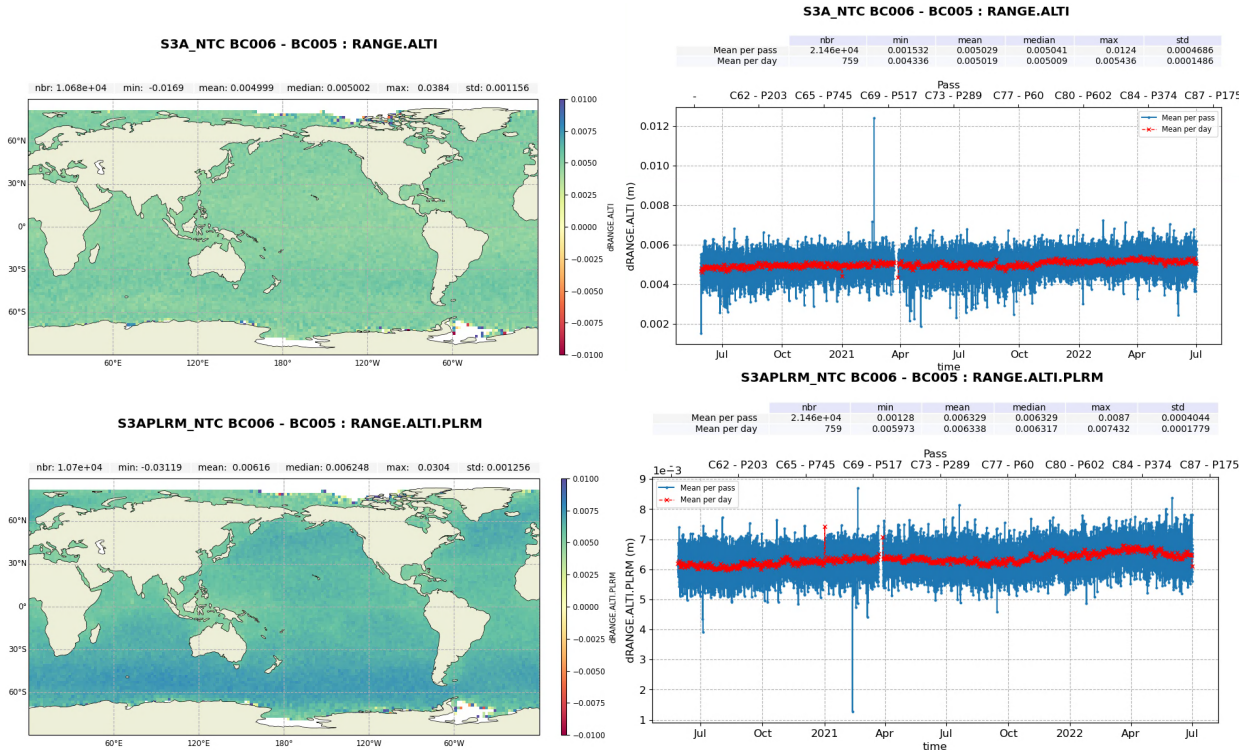

Figure 4: Range difference between BC006.02 and BC005.02 for SAR (top) and PLRM (bottom). Left column: geobox maps of mean difference from June 2020 and June 2022. Right column: time series of mean difference per day (blue) and per pass (red).

with SWH (Figure 5): the reduction is larger in regions characterized by high sea states (i.e. southern ocean), and weak or negligible in regions sheltered by the continents where sea states are smaller. As swells originating from high southern latitudes propagate northward with a small inclination toward East, these regions are north-east of Madagascar, Australia, Hawaii, French Polynesia islands and New Zealand.

Although unexpected, this result is likely due to the combined effects from two of the changes implemented in BC006.02: waveform zero-padding [4] and the new spectral weighting window [3]. Waveform zero-padding is expected to improve the noise level under calm seas, since it doubles the sampling rate and mitigates the occurrence of aliasing artifacts. The new spectral weighting window can act as a low-pass filter smoothing out longer ocean waves and, therefore, can reduce fluctuations in range measurements at high sea states. At the same time, although the causes are not yet well understood, previous studies have shown that it can also increase range noise under calm conditions. The effect of the two corrections can counterbalance each other in sheltered ocean regions, resulting in no variation of range standard deviation.

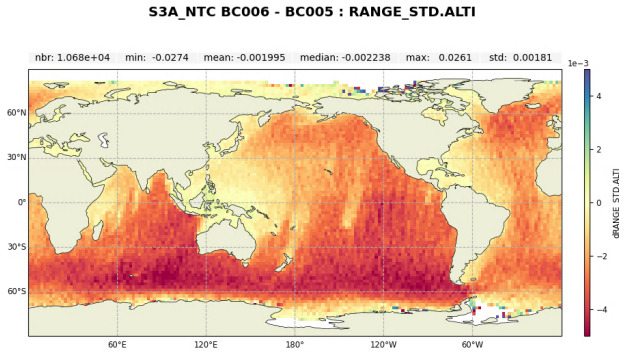

Figure 5: Geobox map of difference in range standard deviation between BC006.02 and BC005.02. As for the mean from the previous figures, the standard deviation is computed over boxes of 2° by 2° for the period June 2020 to June 2022.

However, in the presence of long ocean waves (usually over higher sea states but not only), the weighting window proves beneficial by effectively reducing the range standard deviation. Further investigations will be required to better understand and quantify the role of the two corrections in determining the observed patterns.

3.3. Sigma0

The analysis of sigma0 shows different changes across the two baselines for SAR and PLRM (Figure 6). In SAR mode, sigma0 from BC006.02 is lower than from BC005.02 by 0.02 dB. While fairly stable in time, this bias shows some geographical patterns, with larger values (around -0.05 dB) observed at high latitudes and likely associated with high SWH. In PLRM, the bias between the two baselines is larger (around -0.04 dB) but more spatially homogeneous. However, its temporal evolution is noisier and characterized by a slight positive trend (especially in the earlier months of the time-series). Further studies will be required to better understand its origin and it potential relation to the analogous trend observed for the range (see Figure 4).

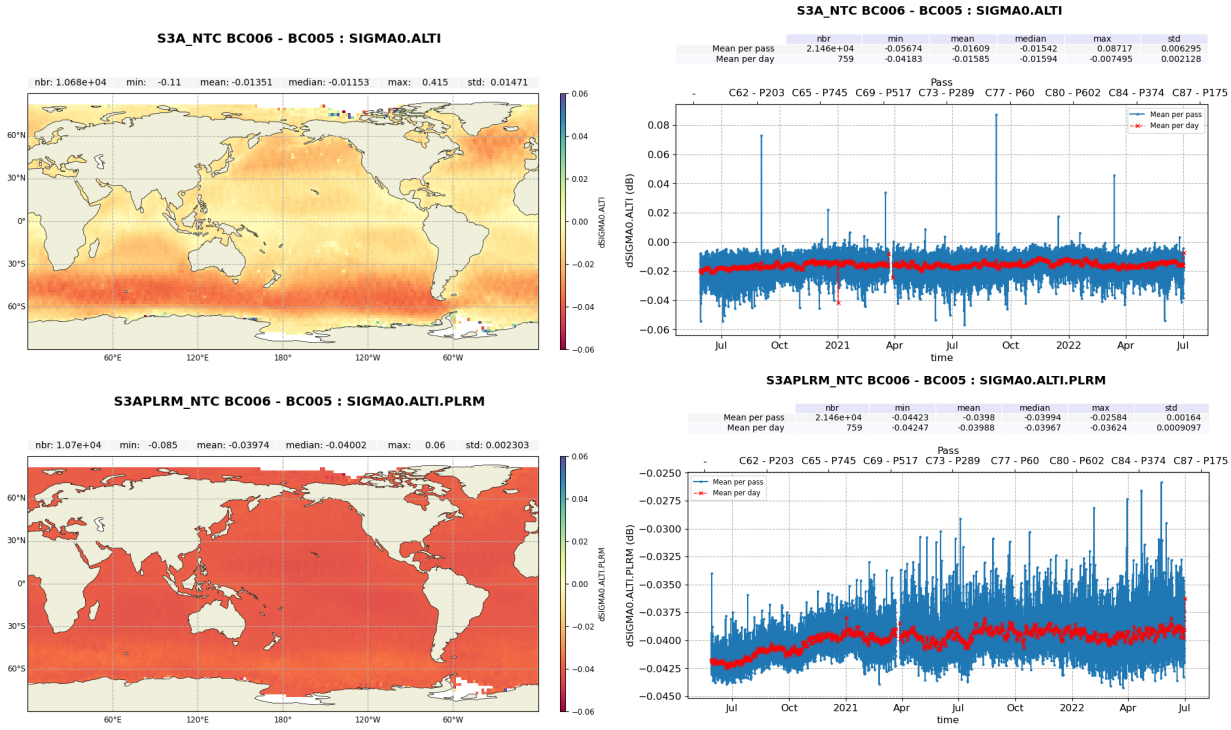

Figure 6: Sigma0 difference between BC006.02 and BC005.02 for SAR (top) and PLRM (bottom). Left column: geobox maps of mean difference from June 2020 and June 2022. Right column: time series of mean difference per day (blue) and per pass (red).

A clear improvement in BC006.02 is observed by comparing the spatial distribution of the sigma0 mode differences (i.e. SAR minus PLRM) between the two baselines (Figure 7). Although positive differences persist at high latitudes, the maps indicate that the latitudinal patterns correlated to the satellite orbital speed observed in BC005.02 have been corrected, and that in BC006.02 SAR and PLRM sigma0 values the equatorial band are more consistent with each other.

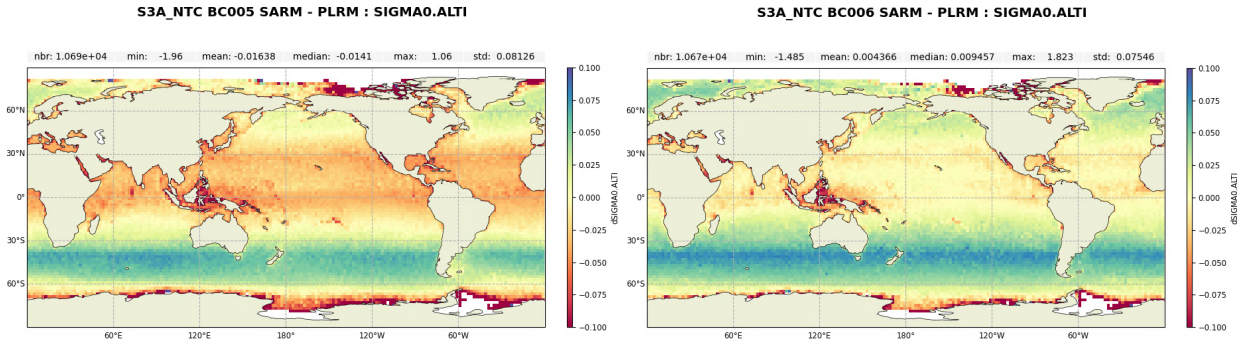

Figure 7: Geobox maps of the mean mode difference (i.e. SAR minus PLRM) of sigma0 for BC005.02 (left) and BC006.02 (right).

3.4. Significant Wave Height

The analysis of SWH shows that the largest differences between the two baselines occur in SAR mode (Figure 8). Values for BC006.02 are consistently lower than for BC005.02 with an average bias of roughly 5 cm. This bias is stable in time, but it is geographically heterogeneous with the larger mean values (reaching up to -15 cm) associated with regions of large waves and strong wind (similar to what observed for sigma0 in Figure 6). The bias in PLRM is much smaller (around 1 cm) and homogeneous in space. The time series of baseline difference shows a drop in values (roughly 2 mm) after October 2021. This is associated with an instrumental discontinuity (variation of the Point Target Response (PTR) main lobe width) which occurred on 1 November 2021. Such instrumental effects were uncalibrated in BC005.02 but are now accounted for by the new calibration scheme implemented in BC006.02.

As for sigma0, another important improvement in BC006.02 is the alignment of SAR and PLRM SWH observations. As shown in Figure 9, the geographical patterns correlated with along-track wind and high

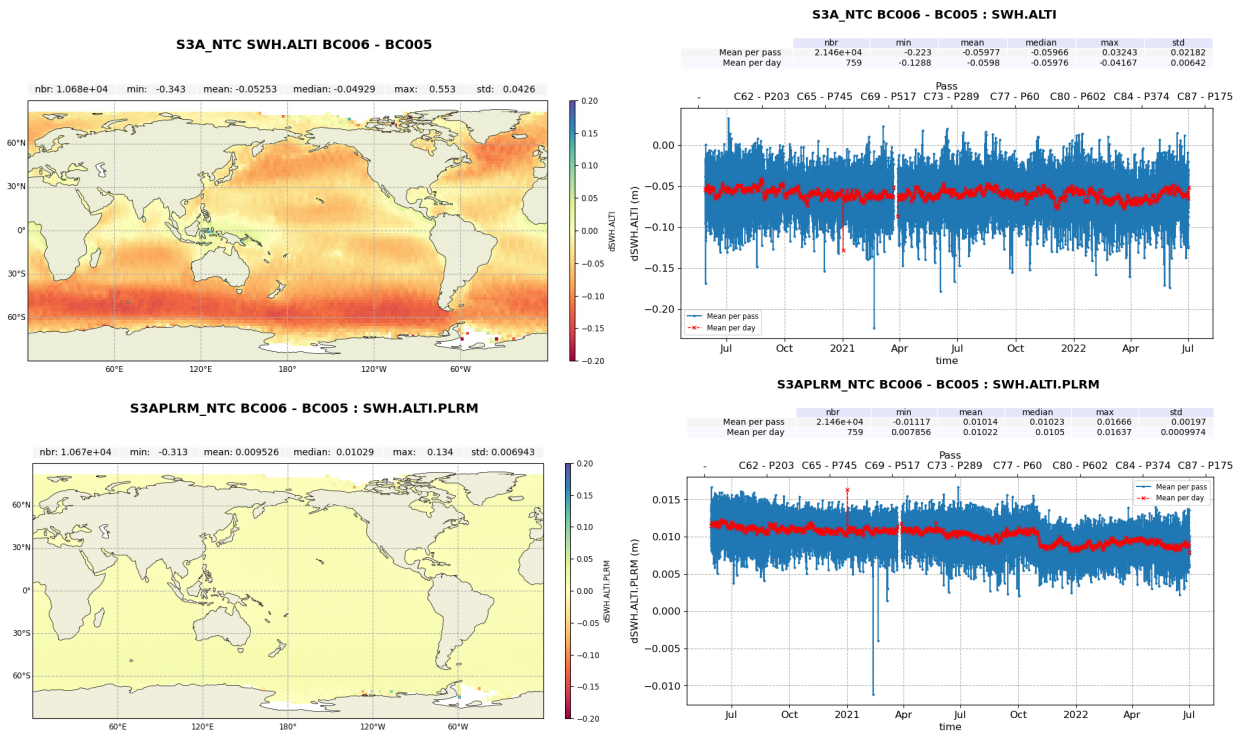

Figure 8: SWH difference between BC006.02 and BC005.02 for SAR (top) and PLRM (bottom). Left column: geobox maps of mean difference from June 2020 and June 2022. Right column: time series of mean difference per day (blue) and per pass (red).

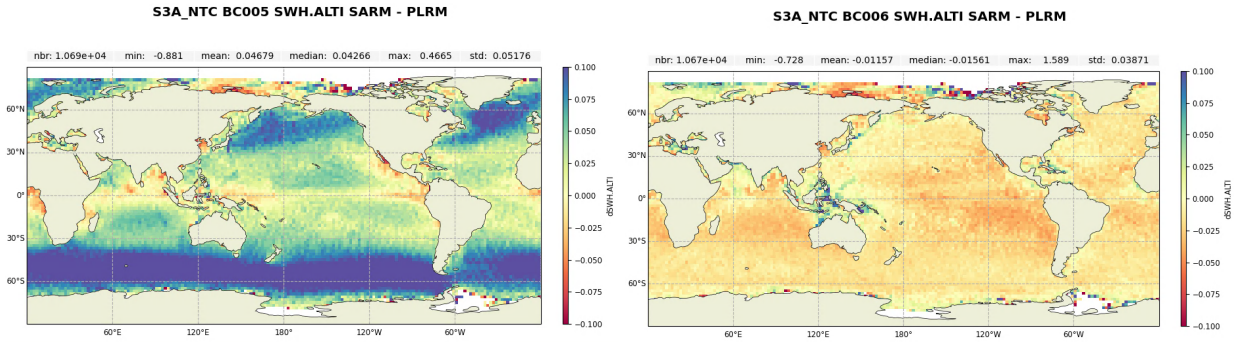

Figure 9: Geobox maps of the mean processing-mode difference (i.e. SAR minus PLRM) of SWH for BC005.02 (left) and BC006.02 (right).

seas that were present in BC005.02 are strongly mitigated in BC006.02.

The BC006.02 product includes 3 new wave field:

- mean_wave_period_t02_alt_01_ku
- wave_sigmav_alt_01_ku
- wave_steepness_alt_01_ku

These were also compared against the equivalent parameters from the ECMWF analysis model. As the results did not show any significant anomaly, they are not included in this report.

3.5. Sea Surface Height Anomaly

SSHA analysis highlighted substantial improvements in open-ocean performance for BC006.02, especially in terms of consistency between SAR and PLRM observations. Bias between the two processing baselines showed similar results for both modes (Figure 10), with SSHA being roughly 0.6 cm smaller on average in BC006.02 than in BC005.02. The difference is stable in time, although showing some small seasonal fluctuations in both mean value and variability. Its geographical distribution shows that the largest values occur over polar regions. These will be discussed in detail in the next section. Outside the polar areas, SSHA differences are mostly homogeneous with some patches of small amplitude variation, particularly in the equatorial band. Detailed analysis of the contribution of the different corrections (not shown here) confirmed that such patterns are due entirely to the different standards used in the two baselines (also consistent with the almost homogeneous maps of range difference from Figure 4).

The comparison of SSHA mode difference between the two baselines puts in evidence reduced values globally in BC006.02 (Figure 11). The bias is almost entirely removed in polar and coastal regions as well as in the south-tropical Indian and Pacific oceans. In the southern ocean, while the latitudinal band of larger different persists, its magnitude is strongly attenuated.

Additionally, the SSHA mode difference was further investigated by comparing ascending and descending passes (Figure 12). In BC005.02, the differences between ascending and descending passes shows regions of large biases equatorward of 40° latitude. The biases are of opposite sign in the two hemispheres. These patterns are well known and are due to errors correlated with along-track winds. The biases are strongly mitigated in BC006.02 indicating improved consistency not only between modes but also between ascending and descending tracks. Some residual patterns remain visible, particularly in the southern ocean. This will be further investigated and corrected in future PB.

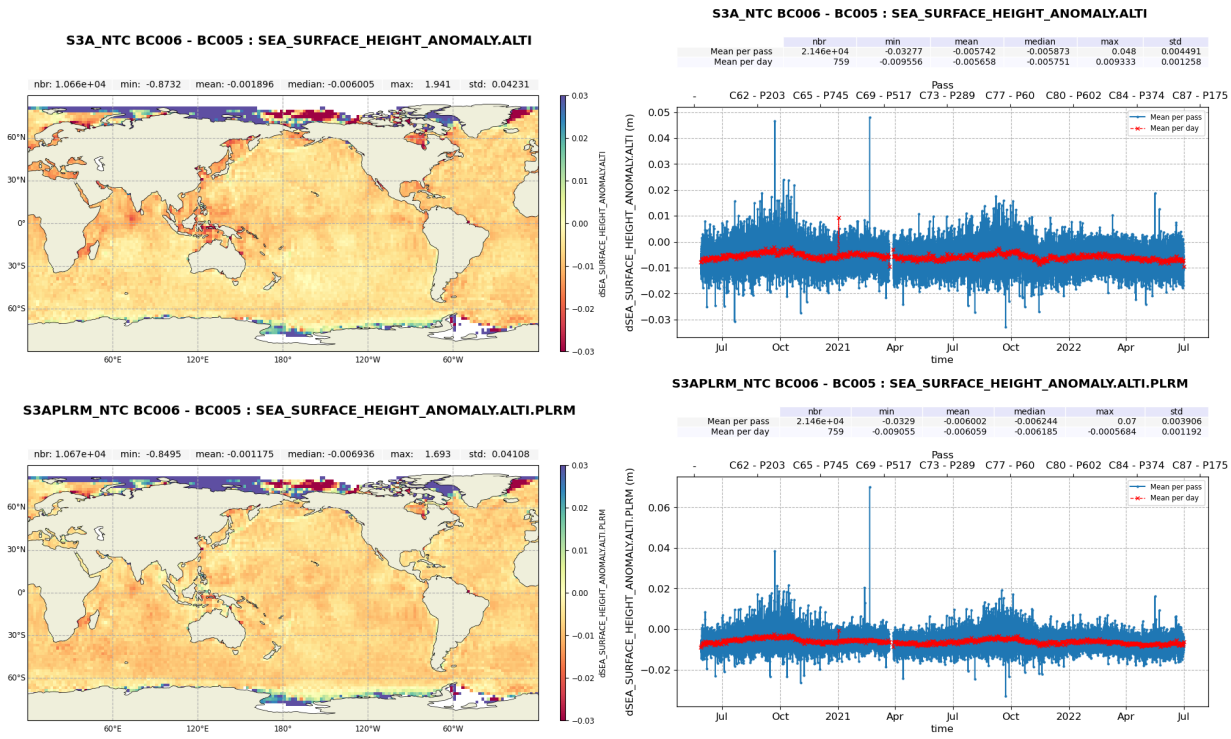

Figure 10: SSHA difference between BC006.02 and BC005.02 for SAR (top) and PLRM (bottom). Left column: geobox maps of mean difference from June 2020 and June 2022. Right column: time series of mean difference per day (blue) and per pass (red).

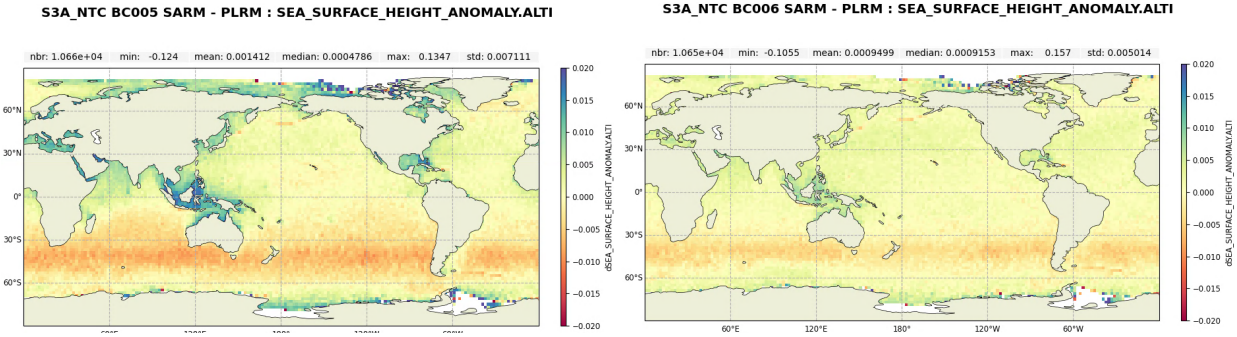

Figure 11: Geobox maps of the mean mode difference (i.e. SAR minus PLRM) of SSHA for BC005.02 (left) and BC006.02 (right).

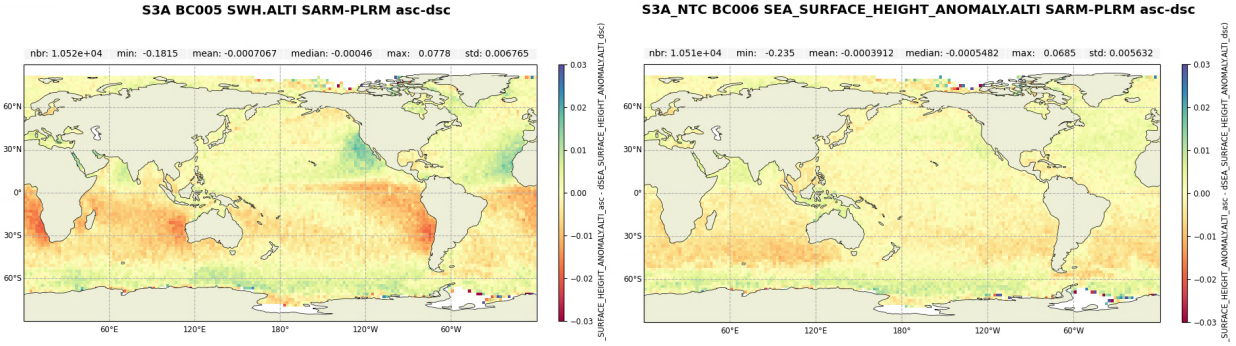

Figure 12: Geobox maps of the mean difference between ascending and descending passes of the mode difference (i.e. SAR minus PLRM) of SSHA for BC005.02 (left) and BC006.02 (right).

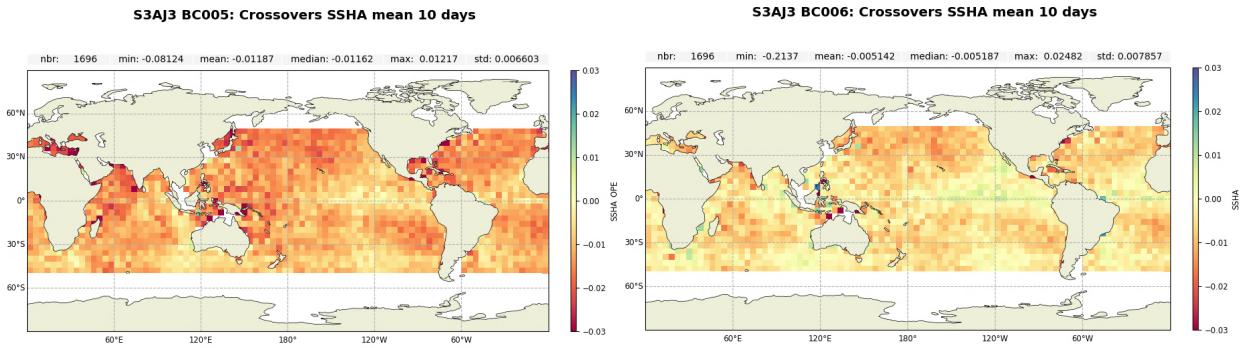

Figure 13: Geobox maps of mean SAR SSHA difference at crossovers between Sentinel-3A and Jason-3 for BC005.02 (left) and BC006.02 (right). The differences were computed only for crossing tracks less than 10 days apart.

SSHA performance was also assessed against the reference missions. Maps of differences at crossovers with respect to Jason-3 (Figure 13) show that BC006.02 remains characterized by similar geographical patterns as observed in BC005.02 but with a more than halved global bias (from -1.1 cm to -0.5 cm). This bias is constant in time with a slightly reduced variability than in BC005.02 (not shown).

The reduced bias with respect to the reference missions was also confirmed by the time series of SSHA daily and 30-day moving mean (Figure 14). The BC006.02 values are much closer to Sentinel-6A and Jason-3, with the bias reduced by 0.6 cm (consistent with the results obtained from the crossover analysis).

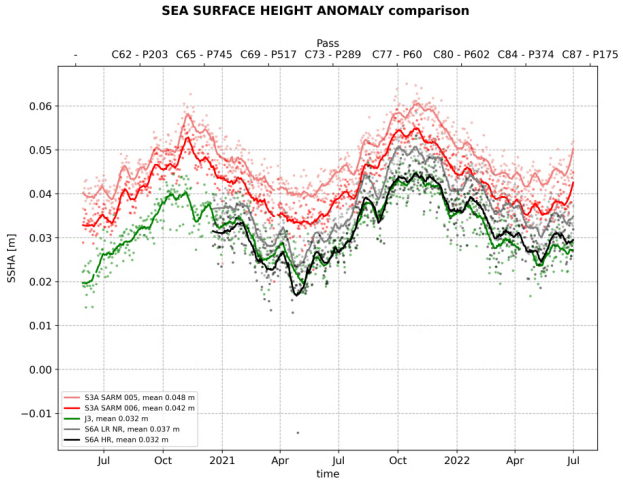

Figure 14: Time series of Sentinel-3 (BC005.02 in light red; BC006.02 in dark red), Sentinel-6A (LR_NR mode in green; HR mode in black) and Jason-3 SSHA (gray). The dots correspond to daily averages; the lines to 30-day moving averages. Sentinel-3 PLRM curves show values analogous to SAR and thus are not shown for figure clarity.

3.6. Spectral Analysis

Power density spectra were computed over continuous along-track segments of 2000 km for both 1 Hz and 20 Hz observations. Before identifying the segments, gaps of 10 consecutive missing and/or invalid observations were linearly interpolated.

SSHA spectra show good consistency between 1 Hz and 20 Hz observations at scales larger than 100 km for both modes (Figure 15). As expected, 1 Hz spectra show higher values at scales below 100 km since the power density is spread over a narrower range of smaller scales than at 20 Hz. Another expected feature is the spectral bump characterizing the PLRM spectra at scales between 15 and 5 km. BC006.02 and BC005.02 are consistent for both modes and at both sampling rates. Small differences between the

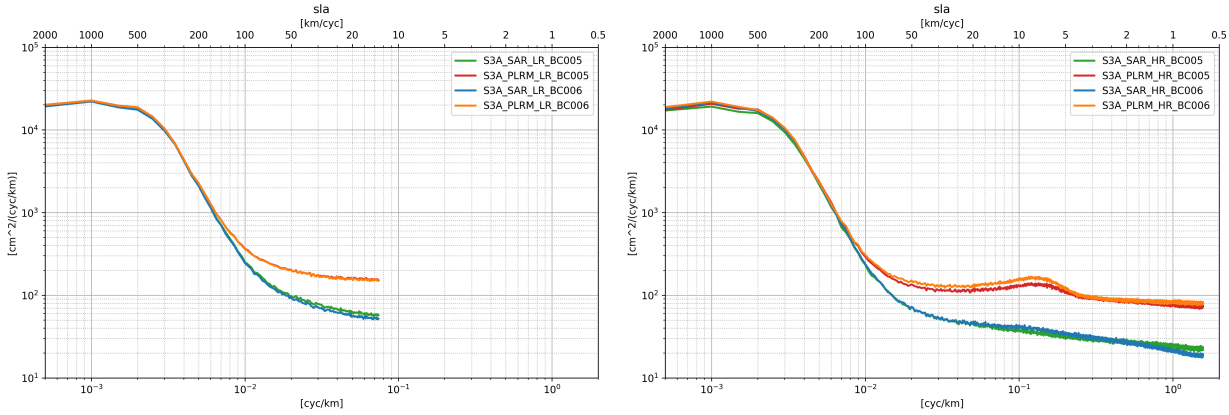

Figure 15: SSHA power density spectra for 1 Hz (left) and 20 Hz observations (right).

two include: for PLRM, slightly higher power density values for BC006.02 at scales smaller than 100 km; for SAR mode, lower power density values for BC006.02 at scales smaller than 2 km (consistent with what observed in Figure 5) and slightly higher values between 5 and 20 km scales. Such bump was already observed for BC004, but it was not present in BC005.02. Further studies will be required to investigate its origin and overall impact in the SSHA performance.

SWH power density spectra were also investigated (Figure 16). Although characterized by different power density levels, the SWH spectra show analogous features as those from Figure 15. The 1 Hz and 20 Hz spectra are analogous for both modes at scales larger than 100 km. Below 100 Km, the PLRM BC006.02 spectra are slightly higher than the BC005.02 one. In SAR mode, the BC006.02 power density is smaller than for BC005.02 at scales below 2 km, and much larger at scales between 2 and 100 km. This increased noise in SWH is an expected drawback of the new spectral weighting window introduced in BC006.02, and it is consistent with the results of the sensitivity analysis reported in [3].

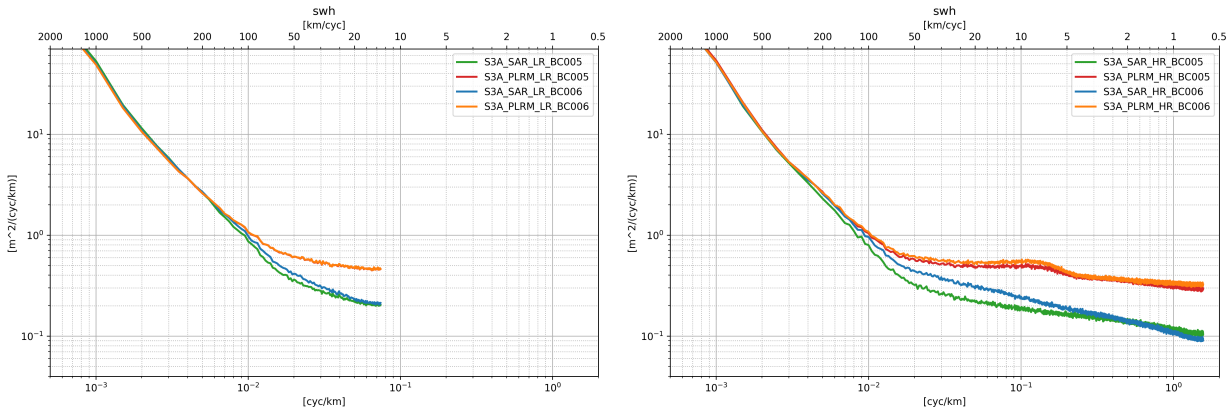

Figure 16: SWH power density spectra for 1 Hz (left) and 20 Hz observations (right).

4 Results: Polar regions

The second part of the cal/val activities focused on the polar regions to assess the improvements in both the quality of Sentinel-3 observations and in the continuity between open and polar ocean following the changes introduced with BC006.02. The analysis focused on 20 Hz observations and on the dedicated polar SSHA variable specifically introduced in the products with the new processing baseline.

4.1. Leads detection

The first assessment of the cal/val analysis in the polar regions was on the leads detected using the new variable provided in the product, i.e. surf_type_class_wfc_20_ku (Figure 17). The variable is based on the waveform classes defined by the neural network classification presented in [9]. Ice leads are represented by one of those classes. Results were compared against leads detected in BC005.02 and those detected in premliminary BC006.02 using the using the previous flag, i.e. surf_type_class_20_ku.

The time-series of daily number of lead observations show that lead detection in BC006.02 is more conservative than in BC005.02. All time series show consistent annual cycles following ice formation and melting. However, the number of leads identified via the new waveform classification variable in BC006.02 is substantially smaller than the ones identified using the previous criteria for both baselines.

The geobox maps show that the reduction occurs throughout both polar regions with little spatial variability. On average, BC006.02 lead detection identifies roughly 20% less leads than BC005.02 in the Arctic and roughly 15% less in the Antarctic. Further analysis (not shown here) have evidenced that while some leads are not properly identified by the BC006.02 criteria, a very large portion of the higher number of leads detected with the BC005.02 criteria corresponds to false positives (i.e. observations detected as leads when they were not) which negatively polluted the overall quality of the data in polar regions. A more refined version of the flag will be implemented in the BC006 version which will be deployed operationally.

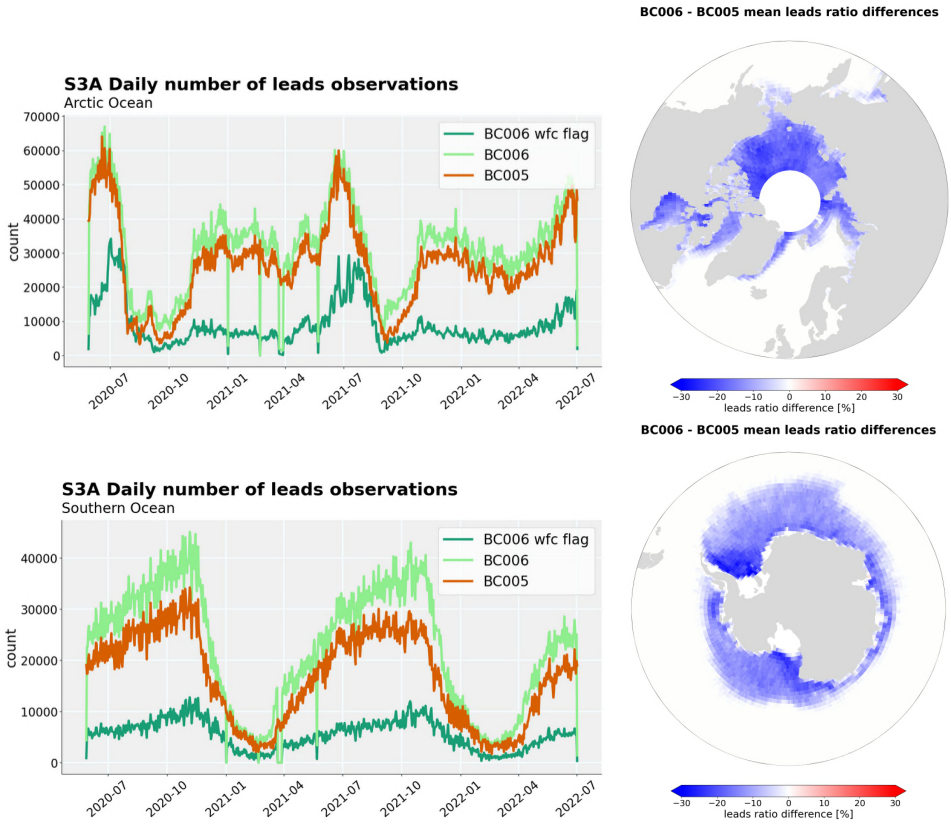

Figure 17: Ice lead analysis in the Arctic (top) and Antarctic regions (bottom). Left column: time-series of daily number of detected leads for BC005.02 (orange), BC006.02 based on the same flag (light green) and BC006.02 based on the new waveform classification flag (dark green). Right column: Geobox maps of the difference in the percentage of leads detected within each box between BC006.02 and BC005.02.

4.2. Sea Level Anomaly

In BC006.02 several changes were introduced to specifically improve the quality of SSHA. In particular:

- Waveform zero-padding to reduce its variability
- The new spectral weighting window to improve the continuity between leads and open ocean
- GDR-G standards (e.g. the new MSS) to further reduce the biases

Furthermore, the new polar SSHA variable is computed using dedicated corrections. Specifically:

- Model ionospheric correction (iono_cor_gim_20_ku) instead of the dual frequency one
- GDP+ wet tropospheric correction (gpd_wet_tropo_cor_20_ku) instead of the one from the microwave radiometer (or model wet tropospheric correction, i.e. mod_wet_tropo_cor_zero_latitude_20_ku, when the GDP+ is not available)

Time series for BC006.02 and BC005.02 show that SSHA retrieved by the two baselines are very similar in mean value and seasonal variability over both polar regions (Figure 18). Those values are well aligned with those from the other reference altimetry missions for the polar regions (i.e. CryoSat-2 and SARAL/AltiKa), especially for the Antarctic ocean. In our analysis, CryoSat-2 SSHA is from the CryoTEMPO dedicated polar ocean product. The differences observed in the Arctic ocean with respect to SARAL/AltiKa are due to a known bias impacting those measurements in that region.

The largest improvements between the two baselines are observed in the geographical distribution of SSHA (Figure 19). In BC006.02 the occurrence of large absolute values of mean SSHA around Greenland and Canada in the Arctic ocean and around the coast and the ice margin zone in the Antarctic ocean are strongly mitigated. Furthermore, the geographical patterns observed in BC006.02 are more consistent with those observed from CryoTEMPO (was well as SARAL/AltiKA, not shown).

Substantial improvements are also observed in terms of SSHA variability (Figure 20). This is greatly re-

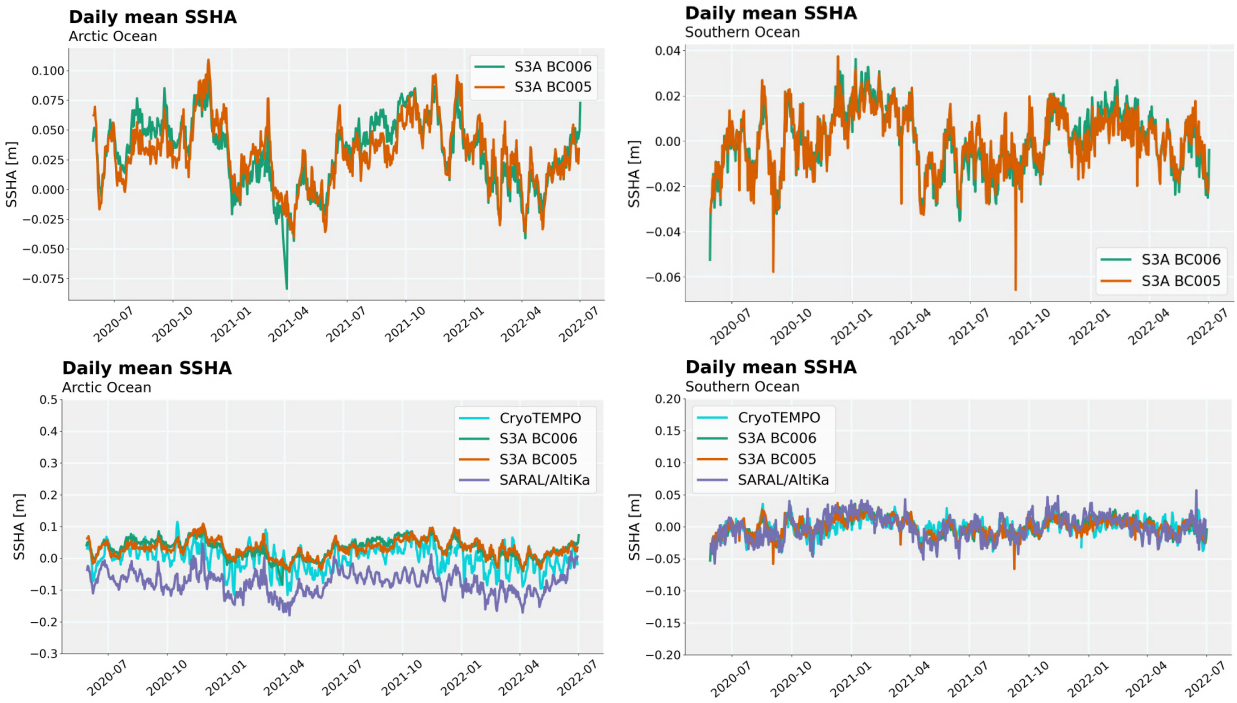

Figure 18: Time series of daily mean SSHA for the Arctic (left column) and Antarctic regions (right column). Top: time-series for BC005.02 (orange) and BC006.02 (green). Bottom: same time series as top but also compared to CryoTEMPO (cyan) and SARAL/AltiKa SSHA (purple).

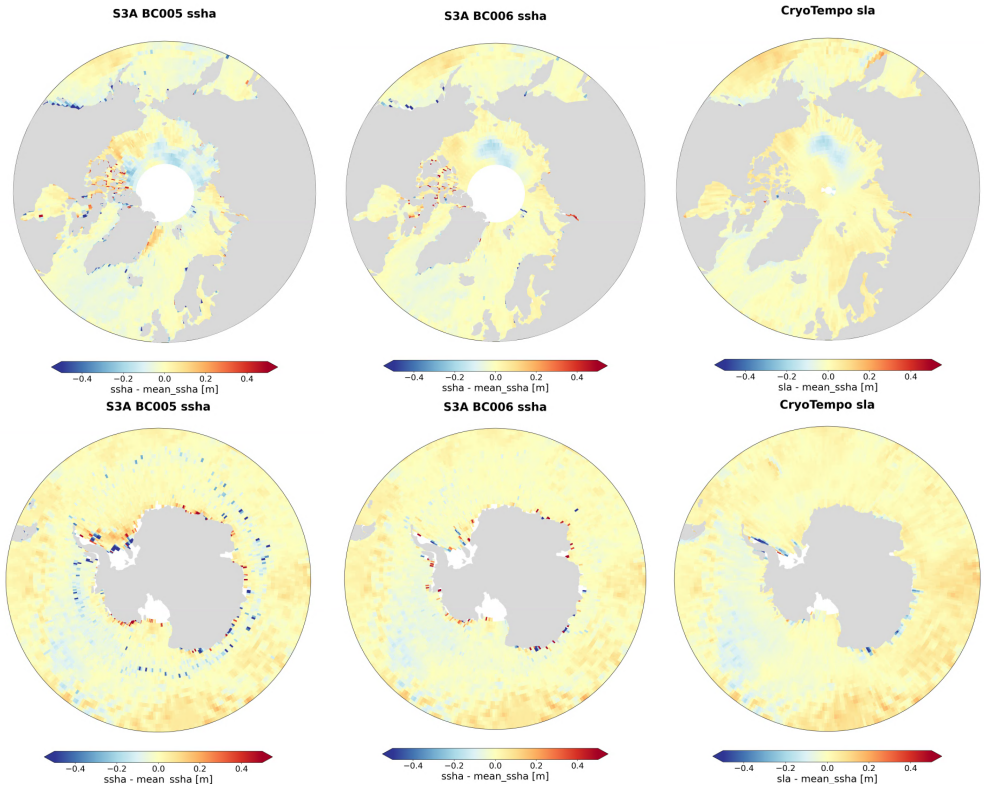

Figure 19: Geobox maps of average SSHA in the Arctic (top) and the Antarctic region (bottom). Left column: BC005.02; Middle column: BC006.02; Right column: CryoTEMPO.

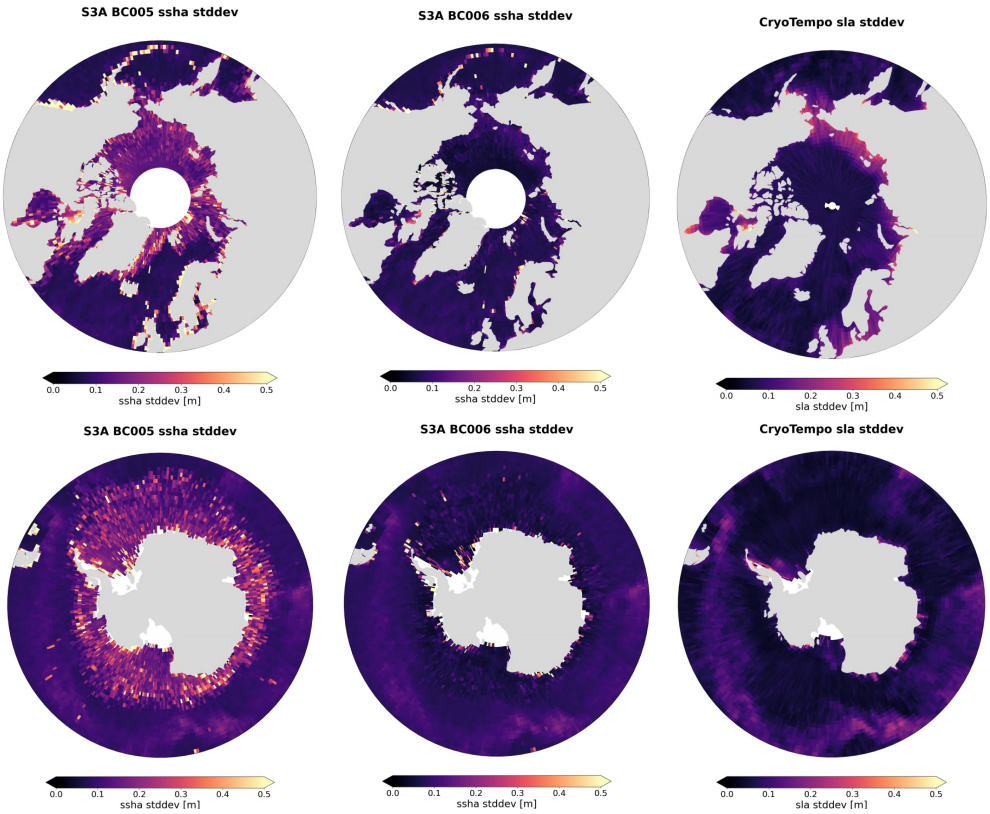

Figure 20: Geobox maps of standard deviation of SSHA in the Arctic (top) and the Antarctic region (bottom). Left column: BC005.02; Middle column: BC006.02; Right column: CryoTEMPO.

duced in BC006.02 with respect to BC005.02 in both polar regions. This reduction results from the combined effect of waveform zero-padding and more conservative lead detection variable (which strongly reduces the number of false positive leads included in the analysis). BC006.02 variability in both polar regions is more consistent with the one observed for the CryoTEMPO products, with a large portion of the residual differences (e.g. along the continent coastlines in the Arctic ocean) likely due to the different correction standards used in the two products.

4.3. Open ocean/lead bias

In our analysis, the open ocean/lead bias is computed by first averaging open-ocean and ice-covered SSHA measurements over common grids independently. The two grids are then subtracted from each other, so that grid cells that have both open-ocean and ice-covered measurements provide one estimate of the bias.

Maps of bias show major improvements in BC006.02, especially in the Antarctic region (Figure 21). The positive biases observed in BC005.02 around the continents in both hemispheres are strongly reduced. The negative bias observed along the ice margin zone in the Antarctic region has been almost entirely removed in BC006.02.

These results are consistent with the time-series of mean bias per cycle (Figure 22). BC006.02 averages are more centered around 0 and characterized by lower variability than BC005.02. This is also confirmed by histograms of mean bias, that are narrower and less skewed (not-shown).

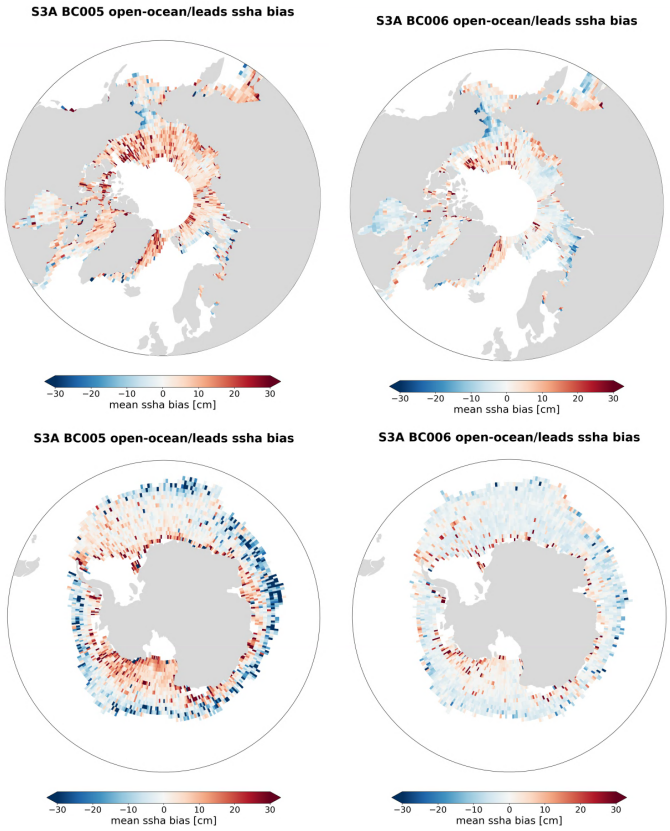

Figure 21: Geobox maps of open-ocean/lead SSHA bias in the Arctic (top) and the Antarctic region (bottom). Left column: BC005.02; Right column: BC006.02.

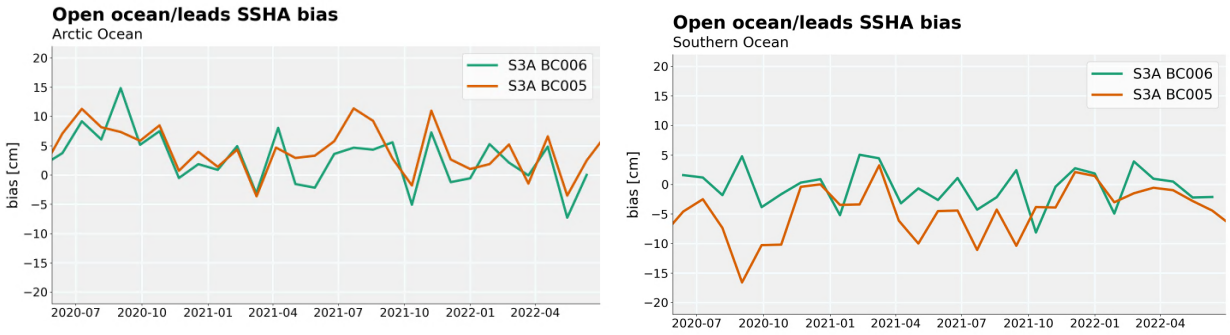

Figure 22: Time-series of mean open-ocean/lead SSHA bias per cycle for the Arctic (left) and the Antarctic regions (right). BC005.02 is in orange; BC006.02 is in green.

5 Conclusions

BC006.02 introduced no regressions with respect to BC005.02 in open-ocean. Performance of open-ocean SSHA has improved over several aspects. The most important include:

- Better consistency between SAR mode and PLRM
- Reduced range noise over high sea conditions
- Removed discontinuities from SWH observations
- Reduced ascending/descending inter-mode track bias due to along-track wind effects
- Better consistency with respect to the reference missions (Jason-3 and Sentinel-6A)

Our results evidenced just a small degradation in SWH observations in the mesoscale range (10 to 100 km scales), which was expected from the new spectral weighting window study.

In polar regions, the changes introduced with BC006.02 lead to:

- Reduced SSHA spikes at coastline and at the edge of sea-covered areas
- Geographical SSHA patterns more coherent with the polar reference missions (CryoSat-2 and SARAL/AltiKa)
- Reduced SSHA variability better aligned with the reference missions (improvement due to waveform zero-padding)
- Mitigated bias between open-ocean and leads (improvement due to the new spectral weighting window)

Our results have shown that the new lead flag based on the new neural-network derived waveform classes is more conservative in detecting leads. However, further comparisons with BC005.02 have shown that a large portion of the reduced number of leads is due to less false positive being detected in BC006.02. Additionally, following up on this assessment, alternative recipes using the output of waveform classification classes were studies by EUMETSAT to further improve the lead detection performance. These will be included in the final release of BC006.

The analysis of edited measurements identified a production bug on the selection of 20 Hz data for compression to 1 Hz. The bug did not have a significant impact on the cal/val results and it will be corrected in the final version of the PB to be deployed in operation.

5.1. Recommendations

Some of the changes observed in BC006.02 remain not completely understood or assessed and should be investigated in more detail in future dedicated studies. These include:

- The dependence of range variability reduction on SWH (and hence on the waveform zero-padding and spectral weighting window effects)
- The significance and origin of the trend in PLRM range difference between the two baselines
- The residual patterns of ascending/descending inter-mode SSHA differences
- The small SSHA spectral bump at around 10 km scales
- An improved lead detection flag for polar regions

Nonetheless, **BC006.02 has shown clear improvements in SSHA performance over both open ocean and polar regions. Such improvements satisfy the needs from the CMEMS over polar ocean (northern and southern) in particular regarding the sea level continuity between the open ocean and polar ocean regions.**

References

[1] EUMETSAT. Copernicus Sentinel-3 Product Notice - STM L1 and L2 Marine (version 3A), March 2023. https://www.eumetsat.int/media/50766.

[2] Salvatore Dinardo, Claire Maraldi, Emeline Cadier, Pierre Rieu, Jeremie Aublanc, Adrien Guerou, Francois Boy, Thomas Moreau, Nicolas Picot, and Remko Scharroo. Sentinel-6 MF Poseidon-4 radar altimeter: Main scientific results from S6PP LRM and UF-SAR chains in the first year of the mission. *Advances in Space Research*, 73(1):337–375, 2024. https://doi.org/10.1016/j.asr.2023.07.030.

[3] Fanny Piras. COPAS: WP 2.1a Magic window Cal/Val Report, CLS-ENV-NT-24-0028, 2024. https://www.eumetsat.int/media/52220.

[4] Graham D. Quartly, Eero Rinne, Marcello Passaro, Ole B. Andersen, Salvatore Dinardo, Sara Fleury, Amandine Guillot, Stefan Hendricks, Andrey A. Kurekin, Felix L. Müller, Robert Ricker, Henriette Skourup, and Michel Tsamados. Retrieving Sea Level and Freeboard in the Arctic: A Review of Current Radar Altimetry Methodologies and Future Perspectives. *Remote Sensing*, 11(7), 2019. https://www.mdpi.com/2072-4292/11/7/881.

[5] Salvatore Dinardo, Ron Abileah, Stefano Vignudelli, Walter Smith, Bruno Lucas, and Remko Scharroo. A Fast-Time Amplitude and Phase Correction for the Global Range Impulse Response of the Sentinel-3 Altimeter, Presentation at 8th S3VT, 2023. https://www.eventsforce.net/eumetsat/frontend/reg/absViewDocumentFE.csp?documentID=1526&eventID=44.

[6] Michel Guerra and Pablo Garcia. COPAS: WP 2.9 AUTOCAL Technical Note, CLS-ENV-NT-24-0568, 2024. https://www.eumetsat.int/media/52316.

[7] EUMETSAT. Copernicus Sentinel-3 Product Notice - STM L1 and L2 Marine (version 3D), December 2024. https://user.eumetsat.int/s3/eup-strapi-media/Copernicus_Sentinel_3_Product_Notice_STM_L1_and_L2_Marine_v3_D_3feda4dfb9.pdf.

[8] Salvatore Dinardo, Luciana Fenoglio-Marc, Christopher Buchhaupt, Matthias Becker, Remko Scharroo, M. Joana Fernandes, and Jérôme Benveniste. Coastal SAR and PLRM altimetry in German Bight and West Baltic Sea. *Advances in Space Research*, 62(6):1371–1404, 2018. https://doi.org/10.1016/j.asr.2017.12.018.

[9] Jean-Alexis Daguze. COPAS: WP 2.1b Waveform Classification: Cal/Val Report, CLS-ENV-RP-24-0566, 2025. https://www.eumetsat.int/media/52519.

[10] Alejandro Egido, Christopher Buchhaupt, François Boy, Claire Maraldi, Cadier Emeline, Dinardo Salvatore, Eric Leuliette, and Thomas Moreau. A Significant Wave Height Correction to Account for Vertical Wave Motion Effects in SAR Altimeter Measurements. In *2022 Ocean Surface Topography Science Team Meeting*, page 193, October 2022. https://doi.org/10.24400/527896/a03-2022.3460.

[11] Salvatore Dinardo, Remko Scharroo, and Bruno Lucas. Towards a reconciliation of the PLRM and SAR altimetry ocean measurements in an operational context for Sentinel-3. In *30 Years of Progress in Radar Altimetry Symposium*, September 2024. https://www.dropbox.com/scl/fi/dt3tjldn4n7og7skybk7i/Session-13.2_Dinardo_30YPRA_v1_0.pdf?rlkey=h62rncirh59biqsrxbc2peq90&e=3&st=omkcdzk4&dl=0.

[12] Ngan Tran. COPAS: WP 2.11 Sea State Bias Validation Performance Report, CLS-ENV-RP-24-0683, 2025. https://www.eumetsat.int/media/52425.

[13] EUMETSAT. Copernicus Sentinel-3 Product Notice - STM L1 and L2 Marine (version 3B), November 2023. https://www.eumetsat.int/media/50766.

[14] Guillaume Dodet. COPAS: WP 2.9 Sentinel-3 SWH LUT, Algorithm Theoretical Basis Document, CLS-ENV-NT-23-0024, 2024. https://www.eumetsat.int/media/52329.

Compliance Matrix

Task	Description	Status
T1Req1	The product fields (20 Hz and 1 Hz) in the test data set shall be ingested in the contractor's internal system in order to carry out thereafter the cal/val analysis. The list of variables to be ingested shall be agreed at Kick-off meeting. At least the following variables shall be assessed (1Hz and 20Hz, SAR and PLRM variants): • range_ocean • ssha • swh_ocean • sig0_ocean • wind_speed_alt_01_ku • sea_state_bias • iono_cor_alt_filtered • rad_wet_tropo_cor • surf_type_class_[wfc]20_ku • *wave*_alt_01_ku The contractor can use other variables considered relevant for the cal/val assessment and non-regression. The 1Hz variables are relative to open ocean region and the 20Hz are relative to polar regions.	Compliant
T1Req2	During the cal/val, the same data editing procedure, used in COPAS cal/val reports (daily report for open ocean case and high-latitude annual report for polar-ocean case), shall be applied to the data	Compliant
T1Req3	A non-regression quality check shall be carried out over open-ocean (Sea Surface Height Anomaly, Wind, Waves, Ionospheric Path Delay, Wet Tropo Correction, Sea State Bias, Sigma0, Range). The cal/val statistical diagnostics to look at shall be: • cross-over maps (mean and std) mono-mission and multi-mission (S6), • time-series (stability), • histograms (data distribution), • scatterplot (data correlation) • geographical maps (mean and difference), • wave-number spectral analysis, • data availability and coverage (number of valid points) • any else suggested by the contractor between processing modes (SAR & PLRM) and versus previous processing baseline. In case of wind and wave, the data quality shall be assessed also with respect to a numerical weather forecast model (ECMWF analysis).	Compliant

Task	Description	Status
T1Req4	Over polar ocean (southern and northern), the contractor shall assess the improvement in data quality brought by BC006.2 by means of a cross-comparison exercise against third-party satellite-based datasets covering the same regions and by means of internal consistency checks. The third-party satellite-based dataset shall be from : • SARAL/Altika mission (GDR-F) • CryoSat-2 mission (ESA Cryotempo) The cal/val statistical diagnostics to look at shall be : • Time-series of the daily mean and diff. ssha (seasonality) • Time-series of number of lead and ocean observations (seasonality) • Geographical mean and std ssha map (geographical variability) • Mean and std map at cross-over (geographical variability) • Estimation of the residual lead/ocean ssha bias between ice-covered and open-ocean regions (continuity) by maps, histogram and time-series • Lead ratio map (mean and difference) • Level of ssha noise (jitter-like) • Data availability and coverage • any else suggested by the contractor The lead shall be identified by means of a dedicated sea-ice lead flag appended in the product. The fieldname of this new flag is surf_type_class_wfc_20_ku. At first, the quality of this new lead-flag shall be assessed and cross-compared versus the heritage one (surface_type_class_20_ku). The polar-ocean ssha fieldname to be used during this cal/val analysis is polar_ocean_20_ku.	Compliant
T1Req5	New wave fields appended in the data products shall be validated over open ocean against the equivalent parameters in the ECMWF analysis model. The fieldnames of these new wave parameters to be used during this cal/val are: • mean_wave_period_t02_alt_01_ku • wave_sigmav_alt_01_ku • wave_steepness_alt_01_ku	Compliant
T1Req6	The contractor shall collect all the requested cal/val diagnostics in a slideshow with a clear description and conclusion. The slideshow shall be made available to EUMETSAT for review before the final delivery.	Compliant

Task	Description	Status
T1Req7	The contractor shall summarize all the main results, findings and conclusions in a brief user-oriented report to be drafted in electronic format and make available to EUMETSAT for review. The report shall also contain recommendations to improve the data quality and a Task1# requirement compliance matrix.	Compliant